Composite Structures 163 (2017) 185–194

Contents lists available at ScienceDirect

Composite Structures

journal homepage: www.elsevier.com/locate/compstruct

Geometrically nonlinear vibration analysis of multiferroic composite plates and shells

S.C. Kattimani

Department of Mechanical Engineering, National Institute of Technology Karnataka, Surathkal 575025, India

ARTICLE INFO

Article history:
Received 1 November 2016
Accepted 5 December 2016
Available online 11 December 2016

Keywords:
Multiferroic composites
Magneto-electro-elastic
Geometrically nonlinear vibrations
Finite element analysis
Composite plates and shells

ABSTRACT

In this article, a layerwise shear deformation theory is incorporated for geometrically nonlinear vibration (GNV) analysis of multiferroic composite plates and doubly curved shells. The coupled constitutive equations involving ferroelastic, ferroelectric and ferromagnetic properties of multiferroic composite materials along with the total potential energy principle are utilized to derive the finite element formulation for the multiferroic or magneto-electro-elastic (MEE) plates/shells. The electric and the magnetic potentials are assumed to vary linearly in the transverse direction. The electric and magnetic potential distribution in the plate/shell is computed by using the Maxwell's electromagnetic relations. The significance of geometric nonlinearity has been considered using the von Kármán nonlinear strain-displacement relations. Importance of curvature aspect ratio, curvature ratio and the thickness aspect ratio on the nonlinear frequency ratios of the multiferroic/MEE doubly curved shells has been investigated. The backbone curves for multiferroic plates and shells have been studied by considering various aspect ratios. Impact of layer stacking sequence, boundary conditions and coupled fields on the central deflection and nonlinear frequency ratio of the multiferroic plates and shells have been investigated.

1. Introduction

Special class of multiphase composite which exhibit the ferroelectric/piezoelectric and magnetostrictive effects are commonly called as multiferroic or magneto-electro-elastic (MEE) composites. These composites have received more attention of the researchers due to their smart properties such as ferroelastic, ferroelectric and ferromagnetic coupling effects. Further, single phase multiferroic composites possess simultaneously more than one energy forms among elastic, electric and magnetic. It is evident from the literature that among the several smart materials, the multiphase composites produced by using the ferroelectric material $BaTiO_3$ (barium titanate) and the ferromagnetic material $CoFe_2O_4$ (cobalt ferrite) can exhibit considerably higher coupling effect in comparison to individual constituent phases [1]. These superior coupling properties of the multiferroic composites may be stimulated the researchers to use these materials in sensors and smart control applications, ultrasonic imaging devices, aeronautical and automotive control systems, sonar applications etc [1–4]. The properties of multiferroic composites can be greatly improved by using layered/laminated form than the bulk/fiber form [3]. On account of these interesting multi behavior properties, the multiferroic/MEE composites gained significant importance in smart structural applications.

The novel research on the electromagnetic effect in mechanical media has attracted the interest of many researchers. The material consisting of piezoelectric and piezomagnetic phases has been developed and studied the effect of elasto-magnetic coupling by Boomgaard et al. [4]. The composite material having the piezoelectric and magnetostrictive properties is developed for the broad band electromagnetic transducer by Bracke and Van [5]. Theoretical and experimental investigation on the electromagnetic composites was investigated by Harshe et al. [6]. Avellaneda and Harshe [7] presented the electromagnetic effect in piezoelectric/magnetostrictive multilayer (2–2) composites. As an early pioneering work, Pan [8] studied the exact solutions of multilayered MEE plates using modified Stroh formalism and propagator matrix method and same approach was extended for free vibration analysis by Pan and Heyliger [9]. Buchanan [10] determined the natural frequencies for MEE infinite plate. Numerous techniques have been applied to examine the free vibration analysis of functionally graded MEE plates/shells, namely, independent state equations by Chen et al. [11], finite element (FE) method by Bhangale and Ganesan [12,13], discrete layer method by Ramirez et al. [14], an asymptotic approach by Tsai et al. [15]. The FE model based on a higher order shear deformation theory for static and free vibration analysis of MEE plates has been developed by Moita et al. [16].

E-mail address: subhaskatti@gmail.com

http://dx.doi.org/10.1016/j.compstruct.2016.12.021
0263-8223/

Making use of three dimensional exact theory, the bending problem of multiferroic rectangular plate with magnetoelectric coupling and imperfect interfaces is investigated by Chen et al. [17]. Wu and Tsai [18] investigated the dynamic responses of functionally graded (FG) MEE shells using the method of multiple scales. Wang et al. [19] studied the transient analysis of multiferroic composite plate by developing a three dimensional finite element formulation and implemented into the software ABAQUS. Lang and Li [20] carried out the buckling and vibration analysis of FG magneto-electro-thermo-elastic circular cylindrical shell by considering the mechanical, electric, magnetic and thermal coupling effects.

Owing to the flexibility, light weight and lower damping properties of multiferroic/MEE composite structures, the dominance of large amplitude vibrations may be observed in the structure. Thus, the influence of geometrical nonlinearity in the composite structure becomes prominent which may lead to instability and progressive or catastrophic failure of the structure. Recently, considerable research on the large amplitude/ large deflection analysis of the MEE plates/ shells has been reported in the literature. Xue et al. [21] demonstrated the analytical solutions for the large-deflection model of rectangular MEE thin plate. They noticed the negligible effect of coupling on the deflection of MEE plate. Sladek et al. [22,23] demonstrated the effect of boundary conditions and layer thickness on multiferroic composites using meshless local Petrov-Galerkin method. Also, they extended the same method for large deformation analysis of MEE thick plates under the static and time-harmonic mechanical load and stationary electromagnetic load. Alaimo et al. [24] proposed an equivalent single-layer model for the large deflection analysis of multilayered MEE laminates by a FE method.

Most recently, Xin and Hu [25] developed the hybrid analysis with combination of the state space approach (SSA) and the discrete singular convolution (DSC) algorithm to study the free vibration of simply supported multilayered MEE plates. Gou et al. [26] investigated the static deformation of anisotropic four layered MEE plates under surface loading based on the modified couple-stress theory. Liu et al. [27] determined the high order solutions for the MEE plates with non uniform materials. Zhou and Zhu [28] used the third order shear deformation theory to study the vibration and bending analysis of multiferroic plates. Further, nonlinear analysis of MEE plates has attracted the interest of researchers considerably. Chen and Yu [29] used the variational asymptotic method to develop the geometrically nonlinear multiphysics plate. Rao et al. [30] proposed the geometrically nonlinear static analysis of multilayered MEE composite structures. Shooshtari and Razavi [31] investigated a nonlinear free and forced vibration of transversely isotropic rectangular MEE thin plate using thin plate theory along with the von Kármán procedure. They extended the same procedure for linear and nonlinear free vibration of multilayered MEE doubly curved shell on elastic foundation [32] and also studied the nonlinear free vibration of symmetric MEE laminated rectangular plate using first order shear deformation theory (FSDT) [33]. Kattimani and Ray [34,35] investigated on the control of geometrically nonlinear vibrations (GNV) of MEE plates and shells using 1–3 piezoelectric composites and later extended their study for FG MEE plates [36]. Further, the comprehensive research on magneto-electro-elastic plates and doubly curved shells has been investigated as doctoral study by Kattimani [37]. Milazzo and his co-workers have been working on the large deflection analysis of magneto-electro-elastic plates using first order shear deformation theory and FE analysis also they have presented smart laminate free vibrations of FG MEE plate using refined equivalent single layer models [38–40]. Farajpour et al. [41] investigated the nonlinear free vibration of size dependent MEE nanoplates subjected to external electric and magnetic potentials by considering the geometrical nonlinearity. In this article, GNV analysis of MEE plates and shells has been investigated. For such investigation, three dimensional FE analysis of the MEE plate/shells has been carried out taking into consideration of electro-elastic and magneto-elastic coupled fields. The effects of different parameters such as the curvature ratio, the curvature aspect ratio, the thickness aspect ratio, the coupling coefficients and the edge boundary conditions on the central deflection and the nonlinear frequency ratios of the MEE plates and doubly curved shells has been studied.

2. Problem description

A schematic representation of multiferroic or magneto-electro-elastic doubly curved shell, the curvature diagram of the paraboloid shell and the hyperboloid shell are illustrated in Fig. 1(a), (b) and (c), respectively. The dimensions of the multiferroic shell are the curvilinear length a, the curvilinear width b and the total thickness *H*. R_1 and R_2 are the radii of curvature of the middle surface. It may be noted that the FE formulation derived here can also be used for the analysis of MEE plates by considering the radii of curvature infinitely large (say $R_1 = R_2 = 2000$). The middle layer of the doubly curved shell is made of ferromagnetic (magnetostrictive) while the bottom and top layer of the shell are made of ferroelectric (piezoelectric). This layer stacking sequence is commonly known as B/F/B indicating B for ferroelectric (Barium titanate) and F for magnetostrictive (Cobalt ferrite). However, the FE formulation derived here can be used for any order of stacking sequence of the multiferroic composite. In the present analysis, the results are obtained for three layered B/F/B and F/B/F layer stacking sequences. The origin of the curvilinear coordinate system (*xyz*) is chosen at one of the corner of the middle-plane of the middle layer of the multiferroic shell such that the curvilinear lines $x = 0$ and a and $y = 0$ and b correspond to the boundaries of the middle-plane of the multiferroic substrate.

2.1. Kinematics of deformations of MEE shell

The multiferroic shell/plate is made of layer of different materials. Hence, to obtain the accurate results, the layerwise shear order

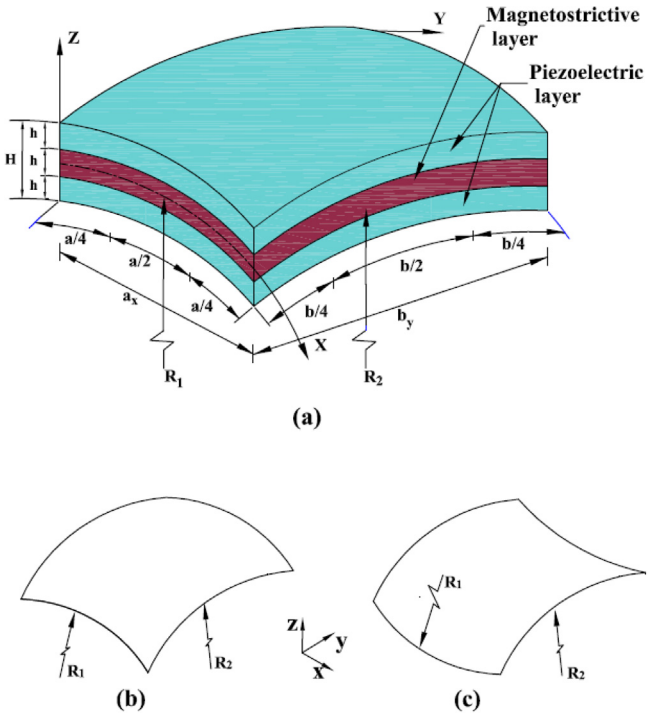

Fig. 1. (a) Schematic diagram of the B/F/B magneto-electro-elastic/multiferroic doubly curved shell (b) curvature of paraboloid shell (c) Curvature of hyperboloid shell.

deformation theory has been incorporated to express the kinematics of deformation of the multiferroic shell. A schematic diagram of the kinematics of deformations of the undeformed transverse normal in the *xz*- and the *yz*-planes are illustrated in Figs. 2(a) and (b), respectively. θ_x and θ_y are the rotations of transverse normal lying in the substrate in the *xz*-plane and in the *yz*-plane, respectively. Consequently, the axial displacements u and v of any point in the doubly curved shell corresponding to the *x*- and the *y*-directions, respectively, may be obtained as follows:

$$u(x,y,z,t) = u_0(x,y,t) + \theta_x(x,y,t),\ v(x,y,z,t) = v_0(x,y,t) + \theta_y(x,y,t) \tag{1a}$$

while for the transverse displacement assumed for the multiferroic shell can be written as

$$w(x,y,z,t) = w_0(x,y,t) + z\theta_z(x,y,t) + z^2\phi_z(x,y,t) \tag{1b}$$

where, u_0, v_0 and w_0 are the translational displacements at any point on the mid-plane of the substrate along *x*-, *y*- and *z*-directions, respectively, while the generalized rotational displacements are θ_z and ϕ_z. To facilitate the computation and evaluation, the displacement variables (rotational $\{d_r\}$ and translational $\{d_t\}$) are separately written as

$$\{d_t\} = [\,u_0 \quad v_0 \quad w_0\,]^T \text{ and } \{d_r\} = [\,\theta_x \quad \theta_y \quad \theta_z \quad \phi_z\,]^T \tag{2}$$

2.2. Strain-displacement relations

The selective integration rule has been utilized to overcome the problem of shear locking in thin structures and computing the element stiffness matrices associated with the transverse shear deformations. To facilitate this task, the in-plane strain vector and transverse shear strains at any point in the multiferroic shell are expressed as

$$\{\varepsilon_b\} = \{\,\varepsilon_x \quad \varepsilon_y \quad \varepsilon_z \quad \varepsilon_{xy}\,\} \text{ and } \{\varepsilon_s\} = \{\,\varepsilon_{xz} \quad \varepsilon_{yz}\,\} \tag{3}$$

The normal strains in Eq. (3) along *x*-, *y*- and *z*-directions are ε_x, ε_y and ε_z, respectively, the in-plane shear strain is ε_{xy}, the transverse shear strains are ε_{xz} and ε_{yz}. The strain vectors defining the state of in-plane and transverse normal strains at any point in the multiferroic doubly curved shell can be expressed using the von Kármán type nonlinear strain-displacement relations as follows:

$$\{\varepsilon_b^k\} = \{\varepsilon_{bt}\} + [Z_n]\{\varepsilon_{rb}\} + \{\varepsilon_{tbn}\};\quad k = 1,2,3,\ldots,N \text{ and } \{\varepsilon_s^k\} = \{\varepsilon_{ts}\} + [Z_s]\{\varepsilon_{rs}\};\quad k = 1,2,3,\ldots,N \tag{4}$$

The transformation matrices $[Z_n]$, $[Z_s]$ and the generalized strain vectors in Eq. (4) for the multiferroic shell are given by

$$Z_n = \begin{bmatrix} z & 0 & 0 & \frac{z}{R_1} & \frac{z^2}{R_1} \\ 0 & z & 0 & \frac{z}{R_1} & \frac{z^2}{R_1} \\ 0 & 0 & 0 & 1 & 2z \\ 0 & 0 & z & 0 & 0 \end{bmatrix}, Z_s = \begin{bmatrix} \left(1-\frac{z}{R_1}\right) & 0 & z & 0 & z^2 & 0 \\ 0 & \left(1-\frac{z}{R_1}\right) & 0 & z & 0 & z^2 \end{bmatrix},$$

$$\{\varepsilon_{bt}\} = \left[\frac{\partial u_0}{\partial x} + \frac{w}{R_1} \quad \frac{\partial v_0}{\partial y} + \frac{w}{R_2} \quad \frac{\partial u_0}{\partial y} + \frac{\partial v_0}{\partial x} \quad 0\right]^T,$$

$$\{\varepsilon_{ts}\} = \left[\frac{\partial w_0}{\partial x} - \frac{u_0}{R_1} \quad \frac{\partial w_0}{\partial y} - \frac{v_0}{R_2}\right]^T.$$

$$\{\varepsilon_{rb}\} = \left[\frac{\partial \theta_x}{\partial x} \quad \frac{\partial \theta_y}{\partial y} \quad \frac{\partial \theta_x}{\partial y} + \frac{\partial \theta_y}{\partial x} \quad \theta_z \quad \phi_z\right],$$

$$\{\varepsilon_{tbn}\} = \frac{1}{2}\left[\left(\frac{dw_0}{dx}\right)^2 \quad \left(\frac{dw_0}{dy}\right)^2 \quad 0 \quad 2\left(\frac{dw_0}{dx}\right)^2\left(\frac{dw_0}{dy}\right)\right]^T \text{ and}$$

$$\{\varepsilon_{rs}\} = \left[\theta_x \quad \theta_y \quad \frac{\partial \theta_z}{\partial x} \quad \frac{\partial \theta_z}{\partial y} \quad \frac{\partial \phi_z}{\partial x} \quad \frac{\partial \phi_z}{\partial y}\right] \tag{5}$$

2.3. Coupled constitutive relations

Similarly, the state of stress at any point in the multiferroic shell can be expressed as:

$$\{\sigma_b\} = [\,\sigma_x \quad \sigma_y \quad \sigma_z \quad \sigma_{xy}\,]^T \text{ and } \{\sigma_s\} = [\,\sigma_{xz} \quad \sigma_{yz}\,]^T \tag{6}$$

in which σ_x ,σ_y and σ_z are the normal stresses along *x*-, *y*- and *z*-directions, respectively; σ_{xy} is the in-plane shear stress; σ_{xz} and σ_{yz} are transverse shear stresses. The coupled constitutive relations for the multiferroic solid substrate are given by

$$\{\sigma_b^k\} = [\bar{C}_b^k]\{\varepsilon_b^k\} - \{e_b^k\}E_z - \{q_b^k\}H_z \text{ and } \{\sigma_s^k\} = [\bar{C}_s^k]\{\varepsilon_s^k\},$$
$$D_z = \{e_b^k\}^T\{\varepsilon_b^k\} + \in_{33}^k E_z + d_{33}H_z, \tag{7}$$
$$B_z = \{q_b^k\}^T\{\varepsilon_b^k\} + d_{33}E_z + \mu_{33}H_z.$$

where, k = 1, 2, 3,. . .,N, D_z, E_z, B_z and H_z are the electric displacement, electrical field, magnetic induction, magnetic field, respectively, along the *z*-direction; $[\bar{C}_b^s]$ and $[\bar{C}_s^s]$ are transformed elastic coefficient matrices; μ_{33} and $\in_{33}^s$ are the magnetic permeability constant and dielectric constant, respectively; d_{33}, $\{e_b^s\}$ and $\{q_b^s\}$ the electromagnetic coefficient, piezoelectric coefficient matrix and the magnetostrictive coefficient matrix, respectively. The assorted matrices shown in Eq. (7) are given by

$$[\bar{C}_b^k] = \begin{bmatrix} \bar{C}_{11}^k & \bar{C}_{12}^k & \bar{C}_{13}^k & \bar{C}_{16}^k \\ \bar{C}_{12}^k & \bar{C}_{22}^k & \bar{C}_{23}^k & \bar{C}_{26}^k \\ \bar{C}_{13}^k & \bar{C}_{32}^k & \bar{C}_{33}^k & \bar{C}_{36}^k \\ \bar{C}_{16}^k & \bar{C}_{26}^k & \bar{C}_{36}^k & \bar{C}_{66}^k \end{bmatrix},\ [\bar{C}_s^k] = \begin{bmatrix} \bar{C}_{55}^k & \bar{C}_{45}^k \\ \bar{C}_{45}^k & \bar{C}_{66}^k \end{bmatrix},$$
$$\{e_b^k\} = \begin{Bmatrix} e_{31} \\ e_{32} \\ e_{36} \\ e_{36} \end{Bmatrix},\ \{q_b^k\} = \begin{Bmatrix} q_{31} \\ q_{32} \\ q_{33} \\ q_{36} \end{Bmatrix} \tag{8}$$

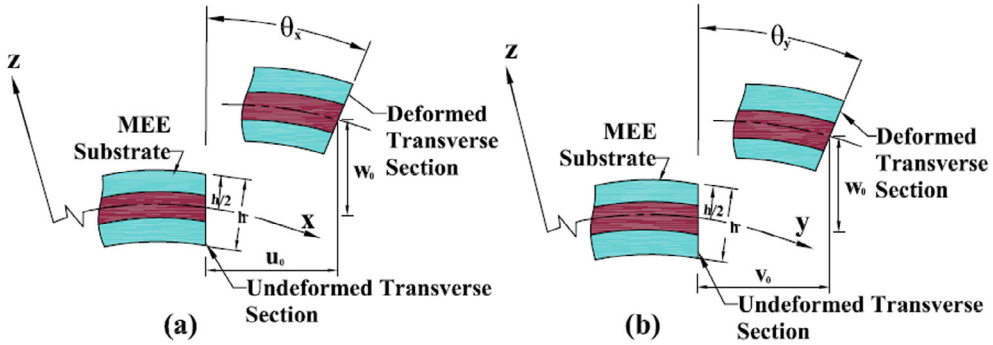

Fig. 2. Kinematics of deformations of the multiferroic shell (a) the transverse cross section parallel to *xz*-plane and (b) transverse cross section parallel to *yz*-plane.

2.4. Electric field-potential relations

Making use of the Maxwell's electromagnetic equations, the transverse electric field in the top layer E_z^t, in the bottom layer E_z^b and the middle magnetic field H_z in case of B/F/B staking sequence of the multiferroic shell are related to the electric potentials ϕ^t and $\phi^b$and the magnetic potential ψ as follows:

$$E_z^t = -\frac{\partial \phi^t}{\partial z}, E_z^b = -\frac{\partial \phi^b}{\partial z} \text{ and } H_z = -\frac{\partial \psi}{\partial z} \tag{9}$$

It should be noted that for very small layer thickness, the variation of the electric potential and the magnetic potential functions may be assumed linear. Also, the interfaces between the ferroelectric layer and the magnetostrictive layer are duly grounded. Consequently, the electric potential functions for the top ferroelectric layer (ϕ^t), the bottom ferroelectric layer (ϕ^b) and the magnetic potential distribution field in the middle ferromagnetic layer (ψ) of the multiferroic composite substrate can be obtained respectively as follows:

$$\phi^t = \frac{z - z_1}{h}\bar{\phi}_1,\ \phi^b = -\frac{z - h_2}{h}\bar{\phi}_2 \text{ and } \psi = \frac{z - h_2}{h}\bar{\psi} \tag{10}$$

where, z_1 and h_2 are the bottom surface of the top piezoelectric layer and the top surface of the bottom piezoelectric layer of the substrate along the z-coordinate, respectively; $\bar{\phi}_1$ and $\bar{\phi}_2$ are electric potentials on the top and the bottom surface of the piezoelectric layer while $\bar{\psi}$ is the magnetic potential on the top surface of the magnetostrictive layer. The thickness of each layer of the substrate is h. It should also be noted that Eqs. (9) and (10) can be augmented for the F/B/F stacking sequence of the multiferroic shell/plate by reinstating the top and the bottom ferroelectric layers with the ferromagnetic layers, while the middle layer is ferroelectric.

3. Finite element formulations for multiferroic shell/plate

The multiferroic substrate shell is discretized by eight noded iso-parametric quadrilateral elements. The size of the mesh for computing the numerical results is considered as 4×4. This results into the total number of translational degrees of freedom as 195 while the total number of rotational degrees of freedom is 520. The principle of virtual work employed to derive the governing equations of the multiferroic shell as follows:

$$\begin{aligned}&\sum_{k=1}^{3}\int_{\Omega^k}\left(\delta\{\varepsilon_b^k\}^T\{\sigma_b^k\} + \delta\{\varepsilon_s^k\}^T\{\sigma_s^k\}\right)d\Omega^k - \int_{\Omega^t}\delta E_z^t D_z^t d\Omega^t \\ &- \int_{\Omega^b}\delta E_z^b D_z^b d\Omega^b - \int_{\Omega^m}\delta H_z B_z d\Omega^m - \int_A \delta\{d_t\}^T\{f\}dA \\ &+ \sum_{k=1}^{3}\int_{\Omega^k}\delta\{d_t\}^T\rho^k\{\ddot{d}_t\}d\Omega^t = 0\end{aligned} \tag{11}$$

$\{f\} = [0\ 0\ p]^T$ is the externally applied surface traction vector acting over a surface area A with p being the transverse step load. Ω^k (k = 1, 2, 3,. . .,N) indicates the volume of the relevant layer, ρ^k is the mass density of the k^{th} layer and δ is the symbol of the first variation. The displacement vectors in general related with the i^{th} (i = 1, 2, 3, . . .,8) node of an element may be written as

$$\{d_{ti}\} = [\,u_{0i} \quad v_{0i} \quad w_{0i}\,]^T \text{ and } \{d_{ri}\} = [\,\theta_{xi} \quad \theta_{yi} \quad \theta_{zi} \quad \phi_{zi}\,]^T \tag{12}$$

The nodal generalized displacement vectors ($\{d_t^e\}$ and $\{d_r^e\}$), the nodal electric potential vector $\{\phi^e\}$ and the nodal magnetic potential vector $\{\bar{\psi}^e\}$ at any point within the element can be written as

$$\begin{aligned}&\{d_t\} = [N_t]\{d_t^e\},\ \{d_r\} = [N_r]\{d_r^e\}, \\ &\{\phi\} = [\,\phi_1 \quad \phi_2\,]^T = [N_\phi]\{\phi^e\} \text{ and } \bar{\psi} = [N_\psi]\{\bar{\psi}^e\}\end{aligned} \tag{13}$$

in which,

$$\begin{aligned}&\{d_t^e\} = [\,\{d_{t1}^e\}^T \quad \{d_{t2}^e\}^T \quad \cdots \quad \{d_{t8}^e\}^T\,]^T,\ \{d_r^e\} = [\,\{d_{r1}^e\}^T \quad \{d_{r2}^e\}^T \quad \cdots \quad \{d_{r8}^e\}^T\,]^T, \\ &\{\phi^e\} = [\,\phi_{11} \quad \phi_{21} \quad \phi_{12} \quad \phi_{22} \quad \cdots \quad \phi_{18} \quad \phi_{28}\,]^T,\ \{\bar{\psi}^e\} = [\,\bar{\psi}_1 \quad \bar{\psi}_2 \quad \cdots \quad \bar{\psi}_8\,]^T, \\ &[N_t] = [\,N_{t1} \quad N_{t2} \quad \cdots \quad N_{t8}\,]^T,\ [N_r] = [\,N_{r1} \quad N_{r2} \quad \cdots \quad N_{r8}\,]^T, \\ &[N_\phi] = \begin{bmatrix} n_1 & 0 & n_2 & 0 & \cdots & n_8 & 0 \\ 0 & n_1 & 0 & n_2 & \cdots & 0 & n_8 \end{bmatrix}^T, \\ &[N_\psi] = [\,n_1 \quad n_2 \quad \cdots \quad n_8\,]^T,\ N_{ti} = n_i I_t,\ N_{ri} = n_i I_r.\end{aligned} \tag{14}$$

where $[N_t]$, $[N_r]$, $[N_\phi]$ and $[N_\psi]$ are the (3×24), (8×64), (2×16) and (1×8) shape function matrices, respectively, I_t and I_r are the (3×3) and the (8×8) identity matrices, respectively and n_i is the shape function of natural coordinates associated with the i^{th} node. Also, ϕ_{1i}, ϕ_{2i} (i = 1, 2, 3, . . .,8) are nodal electric potential degrees of freedom and $\bar{\psi}_i$ (i = 1, 2, 3, . . .,8) are the magnetic potential degrees of freedom. Using Eqs. (9), (10) and (13), the transverse electric fields E_z^t, E_z^b and the transverse magnetic field H_z are given by

$$E_z^t = -\frac{1}{h}[1 \quad 0][N_\phi]\{\phi^e\},\ E_z^b = -\frac{1}{h}[0 \quad 1][N_\phi]\{\phi^e\} \text{ and } H_z = -\frac{1}{h}[N_\psi]\{\bar{\psi}^e\} \tag{15}$$

Now, using Eqs. (4) and (13), the generalized strain vectors at any point within the element can be expressed in terms of the nodal generalized displacement vectors as follows:

$$\begin{aligned}&\{\varepsilon_{bt}\} = [B_{tb}]\{d_t^e\},\ \{\varepsilon_{br}\} = [B_{rb}]\{d_r^e\},\ \{\varepsilon_{tbn}\} = \tfrac{1}{2}[B_1][B_2]\{d_t^e\}, \\ &\{\varepsilon_{st}\} = [B_{ts}]\{d_t^e\} \text{ and } \{\varepsilon_{rs}\} = [B_{rs}]\{d_r^e\}\end{aligned} \tag{16}$$

in which the nodal strain-displacement matrices $[B_{tb}]$, $[B_{rb}]$, $[B_{ts}]$, $[B_{rs}]$, $[B_1]$ and $[B_2]$ are given by

$$\begin{aligned}&[B_{tb}] = [\,B_{tb1} \quad B_{tb2} \quad \cdots \quad B_{tb8}\,],\ [B_{rb}] = [\,B_{rb1} \quad B_{rb2} \quad \cdots \quad B_{rb8}\,], \\ &[B_{ts}] = [\,B_{ts1} \quad B_{ts2} \quad \cdots \quad B_{tb8}\,],\ [B_{rs}] = [\,B_{rs1} \quad B_{rs2} \quad \cdots \quad B_{rs8}\,], \\ &[B_1] = \begin{bmatrix} \dfrac{dw_0}{dx} & 0 & \dfrac{dw_0}{dy} & 0 \\ 0 & \dfrac{dw_0}{dy} & \dfrac{dw_0}{dx} & 0 \end{bmatrix}^T,\ [B_2] = [\,B_{21} \quad B_{22} \quad \cdots \quad B_{28}\,]\end{aligned} \tag{17}$$

The various submatrices $[B_{tbi}]$, $[B_{rbi}]$, $[B_{tsi}]$ and $[B_{rsi}]$ (i = 1, 2, 3, . . ., 8) are clearly demonstrated in Appendix A. On substituting Eqs. (4), (7), (15) and (16) into Eq. (11), the open loop elemental equations of motion for the multiferroic shell are derived as follows:

$$[M^e]\{\ddot{d}_t^e\} + [K_{tt}^e]\{d_t^e\} + [K_{tr}^e]\{d_r^e\} + [K_{t\phi}^e]\{\phi^e\} + [K_{t\psi}^e]\{\psi^e\} = \{F_t^e\} \tag{18}$$

$$[K_{tr}^e]^T\{d_t^e\} + [K_{rr}^e]\{d_r^e\} + [K_{r\phi}^e]\{\phi^e\} + [K_{r\psi}^e]\{\psi^e\} = 0 \tag{19}$$

$$[K_{\phi t}^e]\{d_t^e\} + [K_{r\phi}^e]^T\{d_r^e\} - [K_{\phi\phi}^e]\{\phi^e\} = 0 \tag{20}$$

$$[K_{\psi t}^e]\{d_t^e\} + [K_{r\psi}^e]^T\{d_r^e\} - [K_{\psi\psi}^e]\{\psi^e\} = 0 \tag{21}$$

In Eqs. (18)–(21), the assorted vectors and matrices are $[M^e]$, ($[K_{tt}^e]$, $[K_{tr}^e]$, $[K_{rr}^e]$), ($[K_{t\phi}^e]$, $[K_{r\phi}^e]$), ($[K_{t\psi}^e]$, $[K_{r\psi}^e]$), $[K_{\phi\phi}^e]$, $[K_{\psi\psi}^e]$ and $\{F_t^e\}$ the elemental mass matrix, elastic stiffness matrices, electro-elastic coupling stiffness matrices, magneto-elastic coupling stiffness matrices, electrical stiffness matrix, magnetic stiffness matrix and the elemental mechanical load vector, respectively. The elemental vectors, matrices, stiffness matrices, various rigidity matrices and vectors appearing in Eqs. (19)–(21) are given in Appendix B. These elemental equations of motion are assembled to obtain the coupled global equations of motion of the multiferroic shell/-plate as follows:

$$[M]\{\ddot{X}\} + [K_{tt}]\{X\} + [K_{tr}]\{X_r\} + [K_{t\phi}]\{\phi\} + [K_{t\psi}]\{\psi\} = \{F\}, \quad (22)$$

$$[K_{tr}]^T\{X\} + [K_{rr}]\{X_r\} + [K_{r\phi}]\{\phi\} + [K_{r\psi}]\{\psi\} = 0, \quad (23)$$

$$[K_{t\phi}]^T\{X\} + [K_{r\phi}]^T\{X_r\} - [K_{\phi\phi}]\{\phi\} = 0, \quad (24)$$

$$[K_{t\psi}]^T\{X\} + [K_{r\psi}]^T\{X_r\} - [K_{\psi\psi}]\{\psi\} = 0 \quad (25)$$

where, the mass matrix [M] and the various stiffness matrices $[K_{ii}]$ appearing in Eq. (22)–(25) without superscript *e* represent the global mass matrix and global stiffness matrices, respectively. $\{F\}$ is the global nodal mechanical load vector, $\{X\}$, $\{X_r\}$, $\{\phi\}$ and $\{\psi\}$ are the global generalized nodal displacement vectors, electrical potential and magnetic potential vectors, respectively. Now, applying the boundary conditions and condensation technique to obtain the nodal translational and rotational displacement vectors as follows:

$$[M]\{X_t\} + [K_1]\{X_t\} + [K_2]\{X_r\} = \{F\} \quad (26)$$

$$[K_3]\{X_t\} + [K_4]\{X_r\} = 0 \quad (27)$$

in which, the augmented matrices are given in Appendix C. Further, using Eqs. (26) and (27), the global open-loop equations of motion in time domain are obtained by condensing the rotational degrees of freedom $\{X_r\}$, as follows:

$$[M]\{\ddot{X}_t\} + [K^*]\{X_t\} = \{F\} \quad (28)$$

where,

$$[K^*] = [K_1] - [K_2][K_4]^{-1}[K_3] \quad (29)$$

4. Results and discussions

The finite element (FE) formulation derived in the earlier section is used to analyze the GNV of the multiferroic composite shells/plates. The multiferroic parabolic shell considered for computing the numerical results is shown schematically in Fig.1. The aspect ratio (a/H) of the multiferroic doubly curved shell/plate is considered to be 200. The multiferroic substrate shell is modeled by three layers of equal thickness (h = 0.001 m) with the stacking sequences B/F/B. However, the results are obtained for the stacking sequence F/B/F also. The material properties of $BaTiO_3$ and $CoFe_2O_4$ [8] and BF50% [33] are listed in Table 1. The boundary conditions for the multiferroic plates employed are given in Eq. (30) whereas

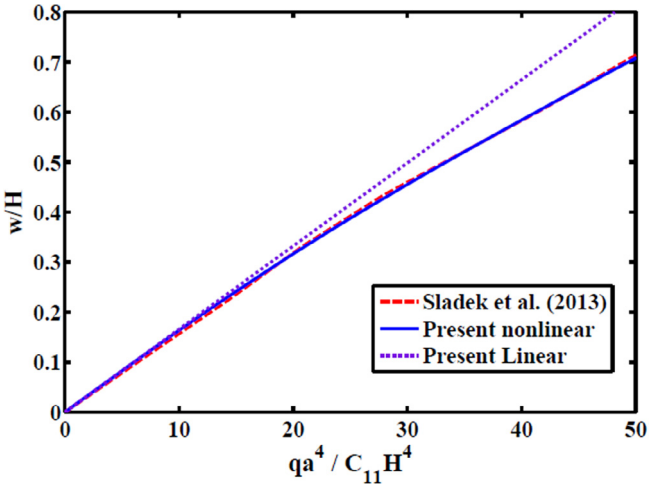

Fig. 3. Central deflection vs. transverse load intensity for a clamped-clamped multiferroic plate/shell ($R_1 = \infty$, $R_2 = R_1$).

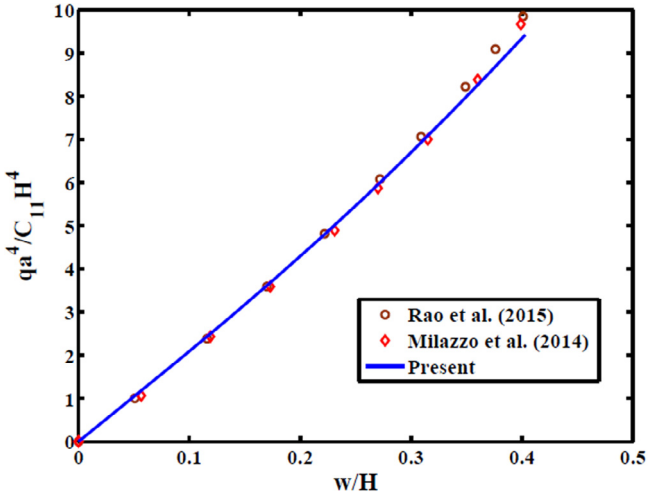

Fig. 4. Central deflection of the plate vs. transverse load intensity for a simply supported multiferroic plate/shell ($R_1 = \infty$, $R_2 = R_1$).

Table 1
Material properties of $BaTiO_3$ and $CoFe_2O_4$ [8].

Material properties with units		$BaTiO_3$	$CoFe_2O_4$	BF50% [30]
$C_{11} = C_{22}$	(10^9 N/m^2)	166	286	213
C_{12}	(10^9 N/m^2)	77	173	113.5
$C_{13} = C_{23}$	(10^9 N/m^2)	78	170.5	112.8
C_{33}	(10^9 N/m^2)	162	269.5	206.5
C_{44}	(10^9 N/m^2)	43	45.3	49.7
C_{66}	(10^9 N/m^2)	44.5	56.5	49.8
$e_{31} = e_{32}$	(C/m^2)	−4.4	0	−2.71
e_{33}	(C/m^2)	18.6	0	8.86
$e_{24} = e_{15}$	(C/m^2)	11.6	0	0.15
$q_{31} = q_{32}$	(N/Am)	0	180.3	222.6
q_{33}	(N/Am)	0	699.7	292.01
$q_{24} = q_{15}$	(N/Am)	0	550	185.13
$\mu_{11} = \mu_{22}$	(10^{-6} Ns^2/C^2)	5	−590	−192.2
μ_{33}	(10^{-6} Ns^2/C^2)	10	157	83.14
$\in_{11} = \in_{22}$	(10^{-9} C2/Nm^2)	11.2	0.08	0.71
$\in_{33}$	(10^{-9} C2/Nm^2)	12.6	0.093	6.32
ρ	(kg/m^3)	1600	1600	1600

in all cases the electric and the magnetic potentials at the boundaries are assumed to be zero.

For simply supported

$$\text{At } x = 0 \text{ and } a;\ v_0 = w_0 = \theta_y = \phi_y = \gamma_y = \theta_z = \phi_z = 0$$
$$\text{At } y = 0 \text{ and } b;\ u_0 = w_0 = \theta_x = \phi_x = \gamma_x = \theta_z = \phi_z = 0 \quad (30a)$$

For clamped-clamped

$$\text{At } x = 0 \text{ and } a; y = 0 \text{ and } b;\ u_0 = v_0 = w_0 = \theta_x = \theta_y = \phi_x = \phi_y = \gamma_y = \theta_z = \phi_z = 0 \quad (30b)$$

4.1. Validation of the FE model

In order to validate the present finite element (FE) formulation, the non-dimensional load parameter $q_0 = qa^4/C_{11}H^4$ is considered to compute the variation of the non dimensional vertical displacement w/H at the center of the multiferroic shell/plate and compared with the results available in the literature [23] for the identical material properties and plate dimensions. The same is illustrated in Fig. 3. In addition, linear solution is also plotted to demonstrate the nonlinear stiffening effect in the plate/shell. It may be noticed that the results are in excellent agreement with each other. To facilitate further validation, the results of the simply supported multiferroic/MEE shell with infinite radii of curvature ($R_1 = \infty$, $R_2 = R_1$) are considered for the comparison with the recently reported results by Milazzo et al. [38] and Rao et al. [30] for the identical geometrical parameters and material properties. Fig. 4 illustrates this comparison for the simply supported MEE plate/shell ($R_1 = \infty$, $R_2 = R_1$). It may also be noticed from this figure (Fig. 4) that the results are in very good agreement.

Table 2
Non dimensional central deflection (w/H) of multiferroic/MEE plate ($R_1 = \infty$, $R_2 = R_1$).

B/F/B						F/B/F			
		Simply Supported		Clamped-clamped		Simply Supported		Clamped-clamped	
a/H	q_0 (Pa)	Linear	Nonlinear	Linear	Nonlinear	Linear	Nonlinear	Linear	Nonlinear
100	100	0.0034	0.0034	0.0022	0.0022	0.0027	0.0027	0.0017	0.0017
	300	0.0102	0.0102	0.0065	0.0065	0.0082	0.0082	0.0052	0.0052
	600	0.0204	0.0204	0.0130	0.0130	0.0164	0.0164	0.0103	0.0103
	900	0.0306	0.0306	0.0195	0.0195	0.0246	0.0246	0.0155	0.0154
	1200	0.0408	0.0407	0.0260	0.0259	0.0328	0.0328	0.0206	0.0205
	1500	0.0510	0.0509	0.0325	0.0324	0.0410	0.0410	0.0258	0.0257
150	100	0.0169	0.0169	0.0102	0.0102	0.0137	0.0137	0.0081	0.0081
	300	0.0508	0.0507	0.0305	0.0304	0.0410	0.0409	0.0244	0.0244
	600	0.1016	0.1008	0.0609	0.0607	0.0820	0.0816	0.0488	0.0487
	900	0.1524	0.1501	0.0914	0.0909	0.1231	0.1219	0.0732	0.0729
	1200	0.2033	0.1984	0.1219	0.1207	0.1641	0.1616	0.0975	0.0970
	1500	0.2541	0.2453	0.1523	0.1503	0.2051	0.2007	0.1219	0.1209
200	100	0.0523	0.0521	0.0294	0.0294	0.0424	0.0423	0.0237	0.0237
	300	0.1570	0.1543	0.0883	0.0878	0.1273	0.1259	0.0712	0.0709
	600	0.3140	0.2984	0.1765	0.1736	0.2545	0.2464	0.1424	0.1409
	900	0.4709	0.4292	0.2648	0.2563	0.3818	0.3592	0.2136	0.2092
	1200	0.6279	0.5483	0.3531	0.3353	0.5515	0.4637	0.2848	0.2756
	1500	0.7849	0.6597	0.4413	0.4104	0.6363	0.5611	0.3560	0.3396

Table 3
Non dimensional central deflection (w/H) of multiferroic doubly curved shell.

B/F/B						F/B/F			
		Simply Supported		Clamped-clamped		Simply Supported		Clamped-clamped	
a/H	q_0 (Pa)	Paraboloid ($R_1 = 10a$, $R_2 = R_1$)	Hyperboloid ($R_1 = 10a$, $R_2 = -R_1$)	Paraboloid ($R_1 = 10a$, $R_2 = R_1$)	Hyperboloid ($R_1 = 10a$, $R_2 = -R_1$)	Paraboloid ($R_1 = 10a$, $R_2 = R_1$)	Hyperboloid ($R_1 = 10a$, $R_2 = -R_1$)	Paraboloid ($R_1 = 10a$, $R_2 = R_1$)	Hyperboloid ($R_1 = 10a$, $R_2 = -R_1$)
100	100	0.00083	0.00339	0.00067	0.00139	0.00074	0.00273	0.00059	0.00116
	300	0.00249	0.01018	0.00202	0.00419	0.00224	0.00819	0.00179	0.00350
	600	0.00498	0.02036	0.00404	0.00837	0.00447	0.01639	0.00357	0.00700
	900	0.00746	0.03053	0.00605	0.01254	0.00670	0.02459	0.00535	0.01049
	1200	0.00993	0.04069	0.00806	0.01671	0.00892	0.03278	0.00713	0.01398
	1500	0.01234	0.05085	0.01006	0.02087	0.01114	0.04096	0.00890	0.01747
150	100	0.00208	0.01683	0.00175	0.01019	0.00192	0.01359	0.00159	0.00408
	300	0.00625	0.05043	0.00525	0.03050	0.00573	0.04077	0.00478	0.01223
	600	0.01246	0.10053	0.01047	0.06072	0.01143	0.08139	0.00953	0.02441
	900	0.01862	0.14998	0.01566	0.09064	0.01710	0.12170	0.01426	0.03654
	1200	0.02475	0.19851	0.02082	0.12025	0.02273	0.16157	0.01896	0.04862
	1500	0.03083	0.24590	0.02594	0.14954	0.02833	0.20088	0.02364	0.06065
200	100	0.00375	0.05158	0.00320	0.01019	0.00348	0.01114	0.00296	0.00900
	300	0.01123	0.15339	0.00959	0.03050	0.01042	0.12509	0.00886	0.02694
	600	0.02236	0.29860	0.01909	0.06072	0.02076	0.24610	0.01765	0.05367
	900	0.03337	0.43145	0.02850	0.09064	0.03101	0.36018	0.02636	0.08018
	1200	0.04428	0.55248	0.03784	0.12025	0.04116	0.46637	0.03500	0.10646
	1500	0.05509	0.66506	0.04709	0.14954	0.05122	0.56526	0.04357	0.13251

4.2. Geometrically nonlinear vibrations (GNV) behavior

The GNV of the multiferroic or MEE shell/plate under a uniform pressure loading is investigated for different aspect ratio (a/H). The non dimensional central deflection versus aspect ratio and the intensity of load for the simply supported and clamped-clamped B/F/B and F/B/F multiferroic plate ($R_1 = \infty$, $R_2 = R_1$) is depicted in Table 2. It evident from this table that with the increase in aspect ratio (a/H) considerable increase in the nonlinear central deflection of a simply supported and clamped-clamped B/F/B and F/B/F plates. The comparison of linear and nonlinear central deflections of the multiferroic plate reveals that the behavior of the plate is almost linear for smaller aspect ratio ($a/H = 100$) while distinguishable nonlinearity has been observed for the higher aspect ratio ($a/H = 200$). It may also be noticed that the central deflection in case of the B/F/B plate is higher than the F/B/F plate. Further, analogous trend has been noticed for the multiferroic doubly curved shells as depicted in Table 3, which illustrates the same for simply supported and clamped–clamped paraboloid ($R_1 = 10a$, $R_2 = R_1$) and hyperboloid ($R_1 = 10a$, $R_2 = -R_1$) multiferroic doubly curved shells. The central deflection of the hyperboloid shells is higher than that of the paraboloid shells for the same geometrical parameters.

4.2.1. Backbone curves and nonlinear dynamics

In order to investigate the dynamic behavior of the multiferroic doubly curved shell/plate, the backbone curves for various aspect ratio and boundary conditions has been considered for the analysis. Consequently, the backbone curves depicting the variation of the frequency ratio (ω_{NL}/ω_L) with the non-dimensional transverse deflection (w_{max}/H) for the simply supported paraboloid ($R_1 = 10a$, $R_2 = 10R_1$) and hyperboloid ($R_1 = 10a$, $R_2 = -10R_1$) multiferroic shells are plotted in Fig. 5. It may be noticed from this figure that the multiferroic/MEE shells display hardening type nonlinearity. It may also be observed from Fig. 5 that for the value of w_{max}/H greater than 0.4, the multiferroic shell exhibits geometrically nonlinear behavior and the nonlinearity increases with increase in frequency ratio (ω_{NL}/ω_L). Fig. 6 illustrates the backbone curves for the simply supported B/F/B and F/B/F multiferroic plates. It is evident from this figure (Fig.6) that the multiferroic plates as well exhibit hardening type nonlinearity. The behavior of the multiferroic plate is linear for the value of non-dimensional transverse deflection (w_{max}/H) is less than 0.2 while turn out be nonlinear for greater than 0.2. In addition, the influence of the curvature ratio (R_1/a) on the response of the nonlinear frequency ratio (ω_{NL}/ω_L) of the spherical ($R_2/R_1 = 1$) multiferroic shell has been presented in

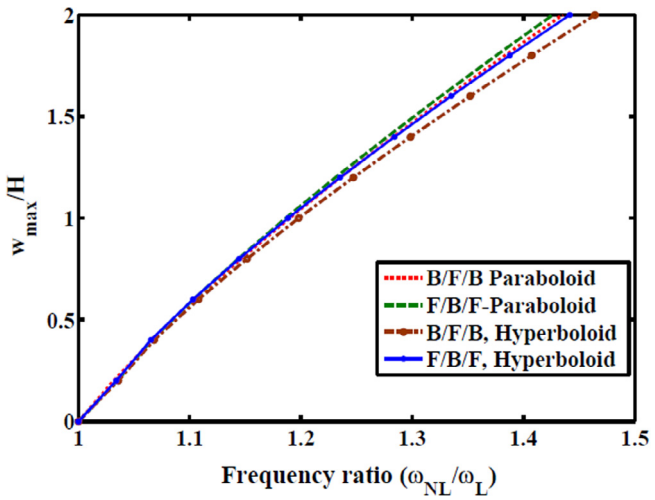

Fig. 5. Backbone curves for the simply supported paraboloid ($R_1 = 10a$, $R_2 = 10R_1$) and hyperboloid ($R_1 = 10a$, $R_2 = -10R_1$) multiferroic doubly curved shells.

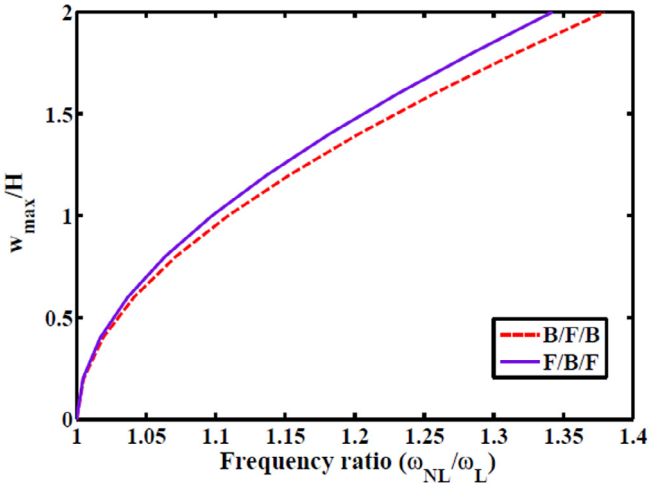

Fig. 6. Backbone curves for the simply supported multiferroic plates ($R_1 = \infty$, $R_2 = R_1$).

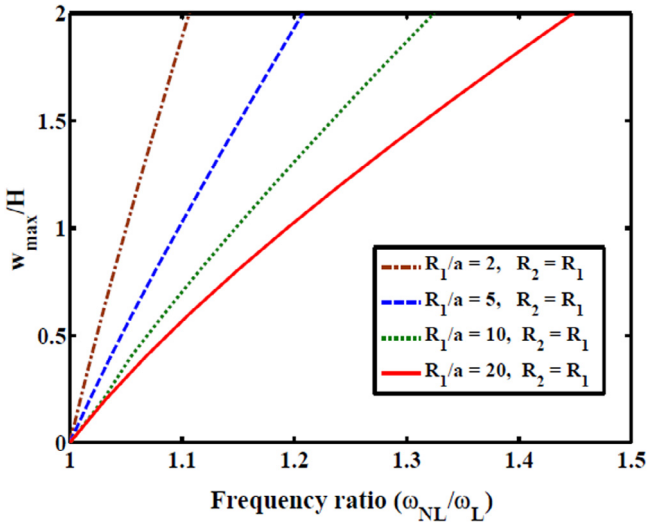

Fig. 7. Influence of curvature ratio (R_1/a) on the nonlinear frequency ratio (ω_{nl}/ω_l) for the simply supported B/F/B-multiferroic doubly curved shells ($a/H = 200$).

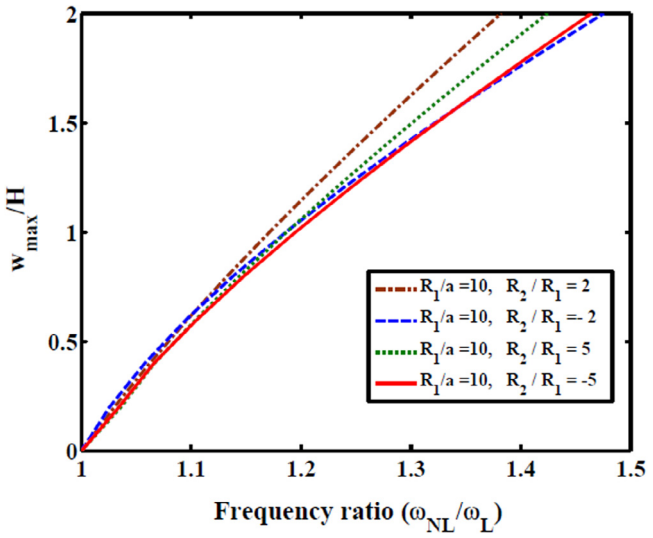

Fig. 8. Influence of curvature aspect ratio on the nonlinear frequency ratio (ω_{nl}/ω_l) for the simply supported B/F/B- multiferroic doubly curved shells ($a/H = 200$).

Fig. 7. It is evident from this figure that the increase in the value of R_1/a increases the hardening type non linearity. Fig. 8 illustrates the effect of the curvature aspect ratio (R_2/R_1) on the frequency ratio (ω_{NL}/ω_L). It may be noticed from Fig.8 that as the amplitude ratio increases, the geometric nonlinearity in the hyperboloid multiferroic shell transforms from softening type to hardening type additionally, the influence of the aspect ratio (a/H) on the fundamental nonlinear frequency ratio (ω_{NL}/ω_L) for the paraboloid and the hyperboloid shells with different stacking sequences have been tabulated in Table 4. It may be seen from this (Table 4) that the frequency ratio increases with the increase in the aspect ratio in both the B/F/B and F/B/F paraboloid shells ($R_2/R_1 = 10$) and hyperboloid shells ($R_2/R_1 = -10$) while this trend is reverse in case of multiferroic plates ($R_1 = 2000a$, $R_1 = R_2$) as depicted in Table 5. It may also be noted that the frequency ratio increases with the increase in the non-dimensional transverse deflection (w_{max}/H) for both MEE plates and shells (Tables 4 and 5).

4.2.2. Effect of coupled fields

The effects of ferro-elastic or electro-elastic and the magneto-elastic couplings may be excluded by setting the stiffness matrices $[K_{t\phi}]$, $[K_{\phi\phi}]$, $[K_{t\psi}]$ and $[K_{\psi\psi}]$ to null matrices. As a result, the responses of the multiferroic composite plate will be free of from these coupling effects. Hence, the effects of coupled fields (ferroelastic/electro-elastic coupling and magneto-elastic coupling) on the frequency ratio (ω_{NL}/ω_L) of a simply supported MEE plate, paraboloid shell and hyperboloid shell for the B/F/B and the F/B/F stacking sequences are tabulated in Table 6. It may be observed from this table that the coupled fields (electro-elastic and magneto-elastic) marginally affect the nonlinear fre-

Table 4
Effect of the aspect ratio (a/H) of the multiferroic paraboloid and hyperboloid shell on the frequency ratio (ω_{nl}/ω_l) of the shells ($R_1/a = 10$).

Layer sequence	Aspect ratio (a/H)	Curvature Ratio	Amplitude ratio (w_{max}/H)				
			0.4	0.8	1.2	1.6	2.0
B/F/B	20	$R_2 = 10R_1$	1.0366	1.1103	1.2102	1.3261	1.4509
		$R_2 = -10R_1$	1.0341	1.1058	1.2044	1.3197	1.4442
	50	$R_2 = 10R_1$	1.0525	1.1367	1.2450	1.3704	1.5073
		$R_2 = -10R_1$	1.0476	1.1285	1.2349	1.3595	1.4964
	100	$R_2 = 10R_1$	1.0672	1.1573	1.2652	1.3861	1.5163
		$R_2 = -10R_1$	1.0623	1.1502	1.2581	1.3808	1.5141
F/B/F	20	$R_2 = 10R_1$	1.0322	1.0974	1.1866	1.2911	1.4042
		$R_2 = -10R_1$	1.0299	1.0934	1.1815	1.2852	1.3981
	50	$R_2 = 10R_1$	1.0467	1.1223	1.2202	1.3343	1.4596
		$R_2 = -10R_1$	1.0423	1.1146	1.2105	1.3236	1.4486
	100	$R_2 = 10R_1$	1.0613	1.1439	1.2433	1.3553	1.4765
		$R_2 = -10R_1$	1.0565	1.1366	1.2355	1.3485	1.4718

Table 5
Effect of the aspect ratio (a/H) of the multiferroic plate on the frequency ratio (ω_{nl}/ω_l) of the plate ($R_1 = 2000a$, $R_1 = R_2$).

Layer sequence	Aspect ratio (a/H)	Amplitude ratio (w_{max}/H)				
		0.4	0.8	1.2	1.6	2.0
B/F/B	20	1.0222	1.0842	1.1760	1.2868	1.4089
	50	1.0210	1.0805	1.1713	1.2856	1.4164
	100	1.0200	1.0764	1.1633	1.2741	1.4027
	200	1.0189	1.0715	1.1529	1.2572	1.3792
F/B/F	20	1.0195	1.0743	1.1561	1.2557	1.3660
	50	1.0186	1.0713	1.1526	1.2554	1.3740
	100	1.0177	1.0679	1.1459	1.2459	1.3629
	200	1.0169	1.0638	1.1368	1.2311	1.3420

Table 6
Effect of the coupled fields on the frequency ratio (ω_{NL}/ω_L) of the multiferroic plate/shell ($a/H = 200$).

Layer sequence		Amplitude ratio (w_{max}/H)				
		0.4	0.8	1.2	1.6	2.0
Plate ($R_1 = 2000a$, $R_1 = R_2$)						
B/F/B	Coupled	1.0189	1.0715	1.1529	1.2572	1.3792
	Uncoupled	1.0190	1.0718	1.1535	1.2585	1.3813
F/B/F	Coupled	1.0169	1.0638	1.1368	1.2311	1.3420
	Uncoupled	1.0168	1.0635	1.1363	1.2303	1.3409
Paraboloid Shell ($R_1 = 10a$, $R_1 = 10R_2$)						
B/F/B	Coupled	1.0669	1.1462	1.2355	1.3325	1.4352
	Uncoupled	1.0686	1.1501	1.2418	1.3414	1.4468
F/B/F	Coupled	1.0659	1.1437	1.2311	1.3259	1.4264
	Uncoupled	1.0644	1.1406	1.2264	1.3195	1.4184
Hyperboloid Shell ($R_1 = 10a$, $R_1 = -10R_2$)						
B/F/B	Coupled	1.0681	1.1515	1.2472	1.3522	1.4643
	Uncoupled	1.0692	1.1542	1.2516	1.3586	1.4728
F/B/F	Coupled	1.0650	1.1444	1.2353	1.3351	1.4417
	Uncoupled	1.0643	1.1430	1.2333	1.3326	1.4387

quency ratio for lower value of the amplitude ratio (w_{max}/H) while the effect is slightly increases for the higher value of (w_{max}/H). It may also be noticed that the value of coupled nonlinear frequency ratios (ω_{NL}/ω_L) are greater in case B/F/B MEE shell/plate than the uncoupled frequency ratio whereas, this trend is reversed for the F/B/F multiferroic plate/shell.

5. Conclusions

In this article, a layerwise shear deformation theory has been incorporated to define the kinematics of deformations the multiferroic/MEE doubly curved shells/plates. The GNV of multiferroic composite plates/doubly curved shells has been analyzed using the finite element analysis by considering the ferroelastic, ferromagnetic and elasto-magnetic coupled fields. The geometric nonlinearity is modeled by using the von Kármán type strain-displacement relations. The nonlinear central deflection increases with increase in aspect ratio of the multiferroic plate/shell. The geometrically nonlinear dynamics of the multiferroic shells/plates are of hardening type. The curvature aspect ratio, the curvature ratio, thickness aspect ratio and boundary conditions exhibit significant influence on the nonlinear behavior of the multiferroic doubly curved shells. For the paraboloid geometry, the multiferroic shells exhibit better stiffening effect than the hyperboloid geometry for the identical material properties. The nonlinear frequency ratio increases with the increase in the aspect ratio of the multiferroic shells for both the B/F/B and the F/B/F paraboloid and hyperboloid shells whereas this trend is reverse in case of multiferroic plates. The coupled fields (ferroelastic and elasto-magnetic) slightly increases the nonlinear frequency ratio for the B/F/B stacking sequence while this trend is reversed for the F/B/F multiferroic plates. The effect of coupled fields is negligible for lower value of amplitude ratio. The present FE model and the comprehensive results presented in this article may provide benchmark problems to future work on the multiferroic or magneto-electro-elastic plates and shells pertaining to geometrically nonlinear vibration analysis.

Appendix A

The various submatrices $[B_{tbi}]$, $[B_{rbi}]$, $[B_{tsi}]$ and $[B_{rsi}]$ (i = 1, 2, 3, ...,8) appearing in Eq. (19) corresponding to MEE shells are as follows:

$$[B_{tbi}]=\begin{bmatrix}\frac{\partial n_i}{\partial x} & 0 & \frac{1}{R_1}\\ 0 & \frac{\partial n_i}{\partial y} & \frac{1}{R_2}\\ \frac{\partial n_i}{\partial y} & \frac{\partial n_i}{\partial x} & 0\\ 0 & 0 & 0\end{bmatrix},[B_{tsi}]=\begin{bmatrix}\frac{-1}{R_1} & 0 & \frac{\partial n_i}{\partial x}\\ 0 & \frac{-1}{R_2} & \frac{\partial n_i}{\partial y}\end{bmatrix},$$

$$[B_{rbi}]=\begin{bmatrix}\hat{B}_{rbi} & \bar{0}\\ \tilde{O} & \bar{I}\end{bmatrix},[B_{rsi}]=\begin{bmatrix}\bar{I} & \tilde{O}\\ \tilde{O} & \hat{B}_{rsi}\\ \tilde{O} & \tilde{B}_{rsi}\end{bmatrix}$$

in which,

$$[\hat{B}_{rbi}]=\begin{bmatrix}\frac{\partial n_i}{\partial x} & 0\\ 0 & \frac{\partial n_i}{\partial y}\\ \frac{\partial n_i}{\partial y} & \frac{\partial n_i}{\partial x}\end{bmatrix},[\hat{B}_{rsi}]=\begin{bmatrix}\frac{\partial n_i}{\partial x} & 0\\ \frac{\partial n_i}{\partial y} & 0\end{bmatrix},[\tilde{B}_{rsi}]=\begin{bmatrix}0 & \frac{\partial n_i}{\partial x}\\ 0 & \frac{\partial n_i}{\partial y}\end{bmatrix}$$

$\bar{0}$ and $\tilde{O}$ are the (3 × 2) and (2 × 2) null matrices, respectively. $\bar{I}$ is the (2 × 2) identity matrix.

Appendix B

The elemental vectors and matrices appearing in Eqs. (19)–(21) are

$$\begin{aligned}&[K^e_{tt}]=[K^e_{tb}]+[K^e_{ts}]+[K^e_{tbn}],\ [K^e_{tr}]=[K^e_{trb}]+[K^e_{trbn}]+[K^e_{trs}],\\ &[K^e_{rt}]=[K^e_{trb}]^T+\tfrac{1}{2}[K^e_{trbn}]^T+[K^e_{trs}]^T,\ [K^e_{rr}]=[K^e_{rrb}]+[K^e_{rrs}],\\ &[K^e_{t\phi}]=[K^e_{t\phi l}]+[K^e_{t\phi n}],\ [K^e_{t\psi}]=[K^e_{t\psi l}]+[K^e_{t\psi n}],\ [K^e_{\phi t}]=[K^e_{t\phi l}]^T+\tfrac{1}{2}[K^e_{t\phi n}]^T,\\ &[K^e_{\psi t}]=[K^e_{t\psi l}]^T+\tfrac{1}{2}[K^e_{t\psi n}]^T,\ \{F^e_{\phi}\}=\{F^e_{1\phi}\}V_1+\{F^e_{2\phi}\}V_2,\\ &\{F^e_{1\phi}\}=\int_0^{a_e}\int_0^{b_e}[1\quad 0]^T[N_\phi]^T\varepsilon_{33}dxdy,\ \{F^e_{2\phi}\}=\int_0^{a_e}\int_0^{b_e}[0\quad 1]^T[N_\phi]^T\varepsilon_{33}dxdy,\\ &\{F^e_{m\psi}\}=\int_0^{a_e}\int_0^{b_e}[N_\psi]^T\mu_{33}dxdy,\ \{F^e\}=\int_0^{b_e}\int_0^{a_e}[N_t]^T\{f\}dxdy\end{aligned}\tag{B1}$$

The elemental stiffness matrices appearing in Eq. (B1) corresponding to the bending stretching deformations are

$$\begin{aligned}&[K^e_{tb}]=\int_0^{a_e}\int_0^{b_e}[B_{tb}]^T[D_{tb}][B_{tb}]dxdy,\ [K^e_{trb}]=\int_0^{a_e}\int_0^{b_e}[B_{tb}]^T[D_{trb}][B_{rb}]dxdy,\\ &[K^e_{rrb}]=\int_0^{a_e}\int_0^{b_e}[B_{rb}]^T[D_{rrb}][B_{rb}]dxdy,\ [K^e_{trbn}]=\int_0^{b_e}\int_0^{a_e}[B_2]^T[B_1]^T[D_{trb}][B_{rb}]dxdy,\\ &[K^e_{tbn}]=\int_0^{a_e}\int_0^{b_e}[\tfrac{1}{2}[B_{tb}]^T[D_{tb}][B_1][B_2]+[B_2]^T[B_1]^T[D_{tb}][B_{tb}]+\tfrac{1}{2}[B_2]^T[B_1]^T[D_{tb}][B_1][B_2]]dxdy,\\ &[K^e_{t\phi}]=\int_0^{a_e}\int_0^{b_e}[B_{tb}]^T[D_{t\phi}][N_\phi]dxdy,\ [K^e_{r\phi}]=\int_0^{a_e}\int_0^{b_e}[B_{rb}]^T[D_{r\phi}][N_\phi]dxdy,\\ &[K^e_{t\phi n}]=\int_0^{a_e}\int_0^{b_e}[B_2]^T[B_1]^T[D_{t\phi}][N_\phi]dxdy,[K^e_{t\psi}]=\int_0^{a_e}\int_0^{b_e}[B_{tb}]^T\{D_{t\psi}\}[N_\psi]dxdy,\\ &[K^e_{r\psi}]=\int_0^{a_e}\int_0^{b_e}[B_{rb}]^T\{D_{t\psi}\}[N_\psi]dxdy,[K^e_{t\psi n}]=\int_0^{a_e}\int_0^{b_e}[B_2]^T[B_1]^T\{D_{t\psi}\}[N_\psi]dxdy,\\ &[K^e_{\phi\phi}]=\int_0^{a_e}\int_0^{b_e}[N_\phi]^T[D_{\phi\phi}][N_\phi]dxdy,\ [K^e_{\psi\psi}]=\int_0^{a_e}\int_0^{b_e}[N_\psi]^T\{D_{\psi\psi}\}[N_\psi]dxdy,\\ &[M^e]=\int_0^{b_e}\int_0^{a_e}\bar{m}[N_t]^T[N_t]dxdy\text{ and }\bar{m}=\sum_{k=1}^{3}\int_{h_k}^{h_{k+1}}\rho^k dz.\end{aligned}\tag{B2}$$

and those associated with the transverse shear deformations are

$$\begin{aligned}&[K^e_{ts}]=\int_0^{a_e}\int_0^{b_e}[B_{ts}]^T[D_{ts}][B_{ts}]dxdy,\ [K^e_{trs}]=\int_0^{b_e}\int_0^{a_e}[B_{ts}]^T[D_{trs}][B_{rs}]dxdy,\\ &[K^e_{rrs}]=\int_0^{b_e}\int_0^{a_e}[B_{rs}]^T[D_{rrs}][B_{rs}]dxdy.\end{aligned}\tag{B3}$$

The various rigidity matrices and rigidity vectors involved in the elemental matrices of Eqs. (B2) and (B3) are given by

$$\begin{aligned}&[D_{tb}]=\sum_{k=1}^{3}\int_{h_k}^{h_{k+1}}[\bar{C}^s_b]^k dz,\ [D_{trb}]=\sum_{k=1}^{3}\int_{h_k}^{h_{k+1}}[\bar{C}^s_b]^k[Z_1]dz,\ [D_{rrb}]\\ &\quad=\sum_{k=1}^{3}\int_{h_k}^{h_{k+1}}[Z_1]^T[\bar{C}^s_b]^k[Z_1]dz,\\ &[D_{ts}]=\sum_{k=1}^{3}\int_{h_k}^{h_{k+1}}[\bar{C}^s_s]^k dz,\ [D_{trs}]=\sum_{k=1}^{3}\int_{h_k}^{h_{k+1}}[\bar{C}^s_s]^k[Z_3]dz,\ [D_{rrs}]\\ &\quad=\sum_{k=1}^{3}\int_{h_k}^{h_{k+1}}[Z_3]^T[\bar{C}^s_s]^k[Z_3]dz,\\ &\{D_{t\psi}\}=\int_{h_2}^{h_3}\{q^s_b\}\tfrac{1}{h}dz,\ \{D_{t\phi}\}=\int_{h_3}^{h_4}\{e^s_b\}\tfrac{1}{h}[1\quad 0]dz+\int_{h1}^{h_2}\{e^s_b\}\tfrac{1}{h}[0\quad 1]dz,\\ &\{D_{r\psi}\}=\int_{h_2}^{h_3}[Z_1]^T\{q^s_b\}\tfrac{1}{h}dz,\ \{D_{r\phi}\}=\int_{h_3}^{h_4}[z_1]^T\{e^s_b\}\tfrac{1}{h}[1\quad 0]dz\\ &\quad+\int_{h1}^{h_2}[z_1]^T\{e^s_b\}\tfrac{1}{h}[0\quad 1]dz,\\ &[D_{\phi\phi}]=\tfrac{\in^s_{33}}{h}\begin{bmatrix}1 & 0\\ 0 & 1\end{bmatrix},\ [D_{\psi\psi}]=\tfrac{1}{h}\mu_{33}\end{aligned}\tag{B4}$$

Appendix C

$$\begin{aligned}&[K_1]=[K_{tt}]+[K_{t\phi}][K_{\phi\phi}]^{-1}[K_{t\phi}]^T+[K_{t\psi}][K_{\psi\psi}]^{-1}[K_{t\psi}]^T,\\ &[K_2]=[K_{tr}]+[K_{t\phi}][K_{\phi\phi}]^{-1}[K_{r\phi}]^T+[K_{r\psi}][K_{\psi\psi}]^{-1}[K_{r\psi}]^T,\\ &[K_3]=[K_{rt}]+[K_{r\phi}][K_{\phi\phi}]^{-1}[K_{\phi t}]^T+[K_{r\psi}][K_{\psi\psi}]^{-1}[K_{\psi t}]^T,\\ &[K_4]=[K_{rr}]+[K_{r\phi}][K_{\phi\phi}]^{-1}[K_{r\phi}]^T+[K_{r\psi}][K_{\psi\psi}]^{-1}[K_{r\psi}]^T.\end{aligned}$$

References

[1] Grossingera R, Giap V, Duongb R, Sato-Turtellia. The physics of magnetoelectric composites. J Magn Magn Mater 2008;320:1972–7.
[2] Wang Y, Yu H, Zheng M, Wan JG, Zhang MF, Liu JM, et al. Numerical modeling of the magneto-electric effect in magnetostrictive piezoelectric bilayer. Appl Phys A 2005;81:1197–202.
[3] Bichurin MI, Filippov DA, Petrov VM, Laletsin VM, Paddubnaya N, Srinivasan G. Resonance magneto-electric effects in layered magnetostrictive-piezoelectric composites. Phys Rev B 2003;68:132408.
[4] Bichurin M, Petrov V, Priya S, Bhalla A. Multiferroic Magnetoelectric Composites and Their Applications. Adv Condens Matter Phys 2012;2012. http://dx.doi.org/10.1155/2012/129794. Article ID 129794, 3 pages.
[5] Bracke LPM, Van VRG. A broadband magnetoelectric transducers using a composite materials. Int J Electron 1981;51:255–62.
[6] Harshe G, Dougherty JP, Newnham RE. Magnetoelectric effect in composite materials. Proc. SPIE 1919, Smart Materials and Structure: Mathematics in Smart Structures 1993;224. http://dx.doi.org/10.1117/12.148414.
[7] Avellaneda M, Harshe G. Magnetoelectric effect in piezoelectric/magnetostrictive multilayer (2–2) composites. J Intell Mater Syst 1994;5:501–13.
[8] Pan E. Exact solution for simply supported and multilayered magneto-electro-elastic plates. ASME Trans 2001;68(4):608–18.
[9] Pan E, Heyliger PR. Free vibrations of simply supported and multilayered magneto-electro-elastic plates. J Sound Vib 2002;252(3):429–42.
[10] Buchanan GR. Layered versus multiphase magneto-electro-elastic composites. Compos B 2004;35:413–20.
[11] Chen WQ, Lee KY, Ding HJ. On free vibration of non-homogeneous transversely isotropic magneto-electro-elastic plates. J Sound Vibr 2005;279:237–51.
[12] Bhangale RK, Ganesan N. Free vibration studies of simply supported non-homogeneous functionally graded magneto-electro-elastic finite cylindrical shells. J Sound Vib 2005;288:412–22.
[13] Bhangale RK, Ganesan N. Free vibration of simply supported functionally graded and layered magneto-electro-elastic plates. J Sound Vib 2006;294:1016–38.
[14] Ramirez F, Heyliger PR, Pan E. Discrete layer solution to free vibrations of functionally graded magneto-electro-elastic plates. Mech Adv Mater Struct 2006;13:249–66.
[15] Tsai YH, Wu CP, Syu SY. Three-dimensional analysis of doubly curved functionally graded magneto-electro-elastic shells. Eur J Mech A/Solids 2008;27:79–105.
[16] Moita JMS, Soares CMM, Soares CAM. Analysis of magneto-electro-elastic plates using higher order finite element model. Compos Struct 2009;91:421–6.
[17] Chen WQ, Zhou YY, Lu CF, Ding HJ. Bending of multiferroic laminated rectangular plates with imperfect interlaminar bonding. Eur J Mech A/Solids 2009;28(4):720–7.
[18] Wu CP, Tsai YH. Dynamic responses of functionally graded Magneto-Electro-Elastic shells with closed-circuit surface conditions using method of multiple scales. Eur J Mech A/Solids 2010;29:166–81.
[19] Wang R, Han Q, Pan E. Transient response ofa bi-layered multiferroic composite plate. Acta Mech Solida Sin 2011;24(1):83–91.
[20] Lang Z, Li X. Buckling and vibration analysis of functionally graded magneto-electro-thermo-elastic circular cylindrical shells. Appl Math Model 2012;37:2279–92.
[21] Xue CX, Pan E, Zhang SY, Chu HJ. Large deflection of a rectangular magnetoelectroelastic thin plate. Mech Res Commun 2011;38:518–23.
[22] Sladek J, Sladek V, Krahulec S, Pan E. Enhancement of the magnetoelectric coefficient in functionally graded multiferroic composites. J Intell Mater Syst Struct 2012. http://dx.doi.org/10.1177/1045389X12449921.
[23] Sladek J, Sladek V, Krahulec S, Pan E. The MLPG analysis of large deflections of magnetoelectroelastic plates. Eng Anal Boundary Elem 2013;37:673–82.
[24] Alaimo A, Benedetti I, Milazzo A. A finite element formulation for large deflection of multilayered magneto-electro-elastic plates. Compos Struct 2014;107:643–53.
[25] Xin L, Hu Z. Free vibration of simply supported and multilayered magneto-electro-elastic plates. Compos Struct 2015;121:344–50.
[26] Guo J, Chen J, Pan E. Static deformation of anisotropic layered magnetoelectroelastic plates based on modified couple-stress theory. Compos B Eng 2016;107:84–96.
[27] Liu J, Zhong P, Gao L, Wang W, Lu S. High order solutions for the magneto-electro-elastic plate with non-uniform materials. Int J Mech Sci 2016;115–116:532–51.
[28] Zhou Y, Zhu J. Vibration and bending analysis of multiferroic rectangular plates using third order shear deformation theory. Compos Struct 2016;153:712–23.
[29] Chen H, Yu W. A multiphysics model for magneto-electro-elastic laminates. Eur J Mech A/Solids 2014;47:23–44.
[30] Rao MN, Schmidt R, Schröder K-U. Geometrically nonlinear static FE-simulation of multilayer magneto-electro-elastic composite structures. Compos Struct 2015;119:377–84.
[31] Shooshtari A, Razavi S. Nonlinear vibration analysis of rectangular magneto-electro-elastic thin plates. IJE Trans A Basics 2015;28(1):136–44.
[32] Shooshtari A, Razavi S. Linear and nonlinear free vibration of multilayered magneto-electro-elastic doubly curved shells on elastic foundation. Compos B Eng 2015;78:95–108.
[33] Razavi S, Shooshtari A. Nonlinear free vibration of magneto-electro-elastic rectangular plates. Compos Struct 2015;119:344–77.
[34] Kattimani SC, Ray MC. Smart damping of geometrically nonlinear vibrations of magneto-electro-elastic plates. Compos Struct 2014;114:51–63.
[35] Kattimani SC, Ray MC. Active control of large amplitude vibrations of smart magneto-electro-elastic doubly curved shells. Int J Mech Mater Des 2014;10:351–78.
[36] Kattimani SC, Ray MC. Control of geometrically nonlinear vibrations of functionally graded Magneto-electro-elastic plates. Int J Mech Sci 2015;99:154–67.
[37] Kattimani SC. Active Control of Geometrically Nonlinear Vibrations of Magneto-Electro-Elastic Plates and Shells (Ph.D. thesis). IIT Kharagpur; 2015. 2015-04, http://www.idr.iitkgp.ac.in/xmlui/handle/123456789/5535.
[38] Milazzo A. Large deflection of magneto-electro-elastic laminated plates. Appl Math Model 2014;38:1737–52.
[39] Alaimo A, Benedetti A, Milazzo A. A finite element formulation for large deflection of multilared magneto-electro-elastic plates. Compos Struct 2014;107:643–53.
[40] Milazzo A. Rifined equivalent single layer formulations and finite elements for smart laminates free vibrations. Compos B Eng 2014;61:238–53.
[41] Farajpour A, Hari Yzdi MR, Ratgoo A, Loghmani M, Mohammadi M. Nonlocal nonlinear plate model for large amplitude vibration of magneto-electro-elastic nanoplates. Compos Struct 2016;140:323–36.